SIMULATION OF IMPREGNAITION TO THE CNT FOREST BY MOLECULAR DYNAMICS METHOD

T. Tajiri[1], R. Matsuzaki[2] and Y. Shimamura[3]

[1]Tokyo University of Science, Chiba, Japan
Email: ttomo1226hiro@yahoo.co.jp
[2]Tokyo University of Science, Chiba, Japan
Email: rmatsuza@rs.tus.ac.jp, Web Page: http://www.rs.tus.ac.jp/rmatsuza/
[3] Shizuoka University, Shizuoka, Japan
Email: tysimam@ipc.shizuoka.ac.jp, Web Page: http://www.ipc.shizuoka.ac.jp/~tysimam/index-e.html

Keywords: CNT, VACNF, Molecular dynamics, Permeability, Flow enhancement

Abstract
The flow rate of water through carbon nanotube (CNT) membranes is remarkably large, and hence, CNT membranes can be applied in various processes. Here, we conducted a molecular dynamic (MD) simulation of introduction of water into between CNTs of CNT membranes, especially vertically arrayed CNT forests (VACNFs). The results showed that the Knudsen number (*Kn*) increased with increasing volume fraction of fiber (V_f), and *Kn* was greater than 10^{-3}, over which flow become slip flow, for each V_f. Further, the permeability increased as the V_f increased in the slip model by the Darcy's law using MD results, while the permeability in the no-slip model predicted by the Hagen–Poiseuille relation decreased. That is, there is a clear divergence of the permeability tendency between the models. Finally, the results also show that it is easier to permeate water as V_f increases.

1. Introduction

Carbon nanotubes (CNTs) have many excellent characteristics such as high thermal conductance, high strength, and chemical stability. Moreover, it is extensively applied with electrical[1-3], structural[4-6] and biometric[7-9] material. Among them, vertically arrayed CNT forests (VACNFs[10]) have attracted great attention; because they can be made on a large scale at low cost by chemical vapor deposition (CVD[11]), and their mesoporous structures have a high potential for use in nanofluidic applications, such as nanofiltration, biosensor and catalyst[12-14]. In the design of these nanofluidic equipment based on CNTs, it is essential to understand and control the interaction between the CNTs and the fluid[12]. For that reason, many investigations of water permeation inside a CNT have been carried out analytically[15-20] and experimentally[21-24]. It has reported that the flow rates of water through a CNT are one to five orders of magnitude greater than those predicted by the continnum-based no-slip Hagen-Poiseuille relation. Furthermore, these flow rates increase as the area of the permeation region decreases. A similar tendency was seen in the experimental results of Byeongho et al.[25], who investigated water permeability outside a CNT in a VACNF.
Although the flow investigations inside a CNT are done analytically and experimentally, no experimental investigations have been done on the outside of a CNT in a VACNF. Thus, in the present study, we simulated the permeation of water outside a CNT in a VACNF, and investigated the flow of water. Here, we used the Gebart model[26] as permeability model of porous medium, which is known for its consistency with experiments and continuum numerical analyses. However, the fluid inside minute porous on a nanolevel involves a high Knudsen number (*Kn*), and the flow turns into a slip flow, which has a velocity in the liquid/solid interface[27]. Thus, there is a possibility that the Gebart equation cannot be applied to a fluid in a nanopore; however this has not been confirmed yet. Our research goal is to verify the application of the Gebart equation by comparing the permeabilities of the Gebart

Excerpt from ISBN 978-3-00-053387-7

equation (no-slip model), derived using a hypothesizing Hagen-Poiseille flow, and the Darcy's law[28] using MD results (slip model), and the verification of flow tendency in a nanopore.
In this paper, we consider the water fluid, which is at an unsaturated state, outside a CNT. Moreover, we show our results as follows; (1) investigation of the Knudsen number (*Kn*); (2) verification of the application of permeability predicted by a no-slip model; and (3) investigation of the divergence between the permeability in a slip model and a no-slip model.

2. Results

2.1. Analytical model and method

The analytical model of permeation ouside the CNT is shown in Fig. 1(a), and we set the CNT with a cap in the center of graphene, and arranged water molecules above the CNT. The CNT diameter is 2.16 nm, and its length is 3.19 nm. We varied the size of the graphene to reach V_f = 0.090, 0.106, 0.188, 0.311, 0.424, 0.505, 0.611 and 0.706. Here, we defined V_f as V_f = (area of CNT) / (area of graphene) in the model of Fig. 1(a). By applying the boundary conditions to the analytical model in Fig. 1(a), we created the VACNF shown in Fig. 1(b) and conducted the permeation outside the CNT.
In the investigation, we conducted an MD simulation using Large-scale Atom Molecular Massively Paralle Simulation (LAMMPS), and permeated water outside a CNT in the VACNF. In the simulation, we used the TIP3P model [29-31] for water and the AMBER96 [32] for the potential function. The viscosity of water is μ = 0.321 mPas at 300 K [27]. The long range Coulomb forces were computed using the particle-particle particle-mesh (PPPM) method [33] and the mean square error was 10^{-4}. The SHAKE method [34] was used to solve the equation of motion in a constraint condition. We controlled the system temperature by solving the Langevin equation of motion [35] in the relaxation calculation and permeating simulation. We used the values listed in table 1 for each parameter in the potential function and and analysis conditions in the relaxation calculation. The permeating simulation conditions are given in table 2.

2.2. Fluid permeation outside CNTs

In the evaluation formula of fluid permeation, we use the permeability in the Darcy's law[28] (eq. (1)) and the Gebart equation[26] (eq. (2)) which are widely used to verify the permeation behavior of a fluid in a porous media. Here, when we calculate the permeability using MD results, we use Darcy's law.

$$u_{MD} = -\frac{K_{MD}}{\phi \mu}\frac{dP}{dz} \tag{1}$$

$$K_G = \frac{8R^2}{57}\frac{(1-V_f)^3}{V_f^2} \tag{2}$$

where u_{MD} is the velocity of fluid permeation into porous media, K_{MD} is the permeability, μ is the viscosity of a fluid, φ is the porosity, dP/dz is the pressure gradient in the flow direction, K_G is the permeability of the case that the permeation direction is parallel to the fibrous direction, R is the fiber radius and V_f is the volume fraction of a fiber. Then, we consider eq. (1) to be the permeability of a no-slip model, and eq. (2) to be that of a slip model. We compare the permeability obtained from eq. (1) using MD simulation with the one from eq. (2). Furthermore, we calculated dP/dz by evaluating the pressure within several sub-volumes along the CNT axis and performing a linear regression analysis. Here, in the MD we calculate the pressure using virial theorem (eq. (3)) [36].

$$P = \frac{N k_B T}{V} + \frac{1}{3V}\left\langle \sum_{i>j}^{N}\sum^{N} \mathbf{r}_{ij}\cdot\mathbf{F}_{ij} \right\rangle,\ \mathbf{r}_{ij} = \mathbf{r}_i - \mathbf{r}_j \tag{3}$$

where V is the volume, N is the number of atoms, k_B is the Boltzmann constant, T is the temperature, $\mathbf{r}_{ij}$ is the distance between atom i and j, $\mathbf{F}_{ij}$ is the interaction force beween atom i and j.
Then, *Kn* is defined as the ratio of the mean free path and the characteristic length, and it is used to

Excerpt from ISBN 978-3-00-053387-7

determine whether a flow field can be a continuum[37]. We use eq. (4) to determine *Kn* on permeation outside the CNT.

$$Kn = \frac{\lambda}{h'} = \frac{k_B T}{\sqrt{2}\, p\, (4\pi r'^2)} \frac{V_f}{2(1-V_f)R} \tag{4}$$

where λ is the mean free path, *h'* is the characteristic length, and *r'* is the molecular radius. In this paper, we use $k = 1.38 \times 10^{-23}$ J/K and *r'* = 0.19 nm. *h'* is the hydraulic diameter considering the control volume (Fig. 2(c)) of the model where the CNTs stand close together and straight on the substrate (Fig. 2(b)).

2.3. Results of MDS and calculation

We show the results of the MD simulation and the calculation in Fig. 3. First, In Fig. 3(a), *Kn* is higher than 0.001 for each V_f, thus it is found that the water flow becomes slip flow. Furthermore, *Kn* increases as the permeation area becomes narrower. Then, Fig. 3(b) shows the relationship between V_f and permeability (log*K*). In this graph, although the permeability of the slip state using MD results increase, that of no-slip state decreases as the permeating area becomes narrower. On the other hand, the permeability of the slip state using the MD results corresponds with that of the no-slip state as the permeation area becomes wider, that is, the influence of slip becomes smaller.

2.4. Discussion

First, by the tendency of the Fig. 3(b), we can say that there is a clear divergence of the permeability tendency between the slip and no-slip states and the permeabilities show an opposite tendency with V_f. The tendency that the permeability increases and fluid flows more easily as the permeation area becomes narrower, corresponds with the experimental results of Byeongho et.al.[25], who investigated water permeability in a VACNF. On the other hand, the permeability of the slip state corresponds with that of the no-slip state as the permeation area becomes wider. According to the above results, in permeation in nanopore-based CNTs, there exists a wide region where permeability in the no-slip state cannot be applied; therefore it is necessary to consider a new permeability equation with slip. Furthermore, it is found that the V_f increases and water become permeates more easily. This is because almost no friction is generated by the super-hydrophobicity of the CNT. Moreover, there are weak interfacial forces between the CNT and the water molecules.

3. Conclusions

In this study, we conducted a MD simulation of introduction of water into CNT membranes, especially a VACNF. As a result, we acquired the following results. First, *Kn* increased as the permeation area become narrower. Moreover, for each V_f, *Kn* was greater than 10^{-3} where the flow becomes slip flow. Next, while the permeability of the slip state from the MD results increases, that of the no-slip state decrease as the permeating area becomes narrower. On the other hand, the permeability of the slip state using the MD results corresponds with that of the no-slip state as the permeation area becomes wider, that is, the influence of slip becomes smaller. Thus, we can conclude that there is a clear divergence of permeability tendency between the slip state and the no-slip state, and the permeabilities show an opposite tendency with V_f. Furthermore, it is found that the V_f reases and water permeates more easily owing to the influence of the super-hydrophobicity of the CNT and the weak interfacial forces between the CNT and the water molecules..

Excerpt from ISBN 978-3-00-053387-7

Figures

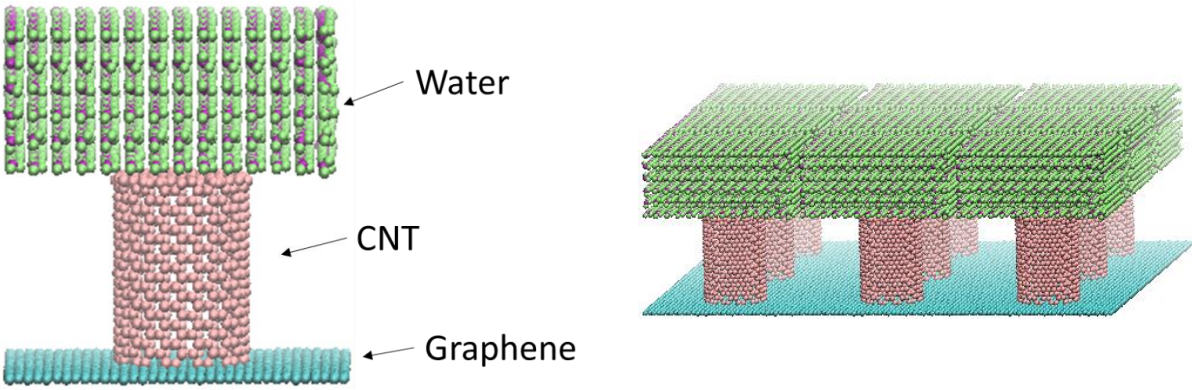

(a) (b)

(c)

Fig. 1 Analytical models and permeating behavior. (a) Analytical model of impregnation outside a CNT. (b) Impregnation is performed by applying the periodic boundary condition.

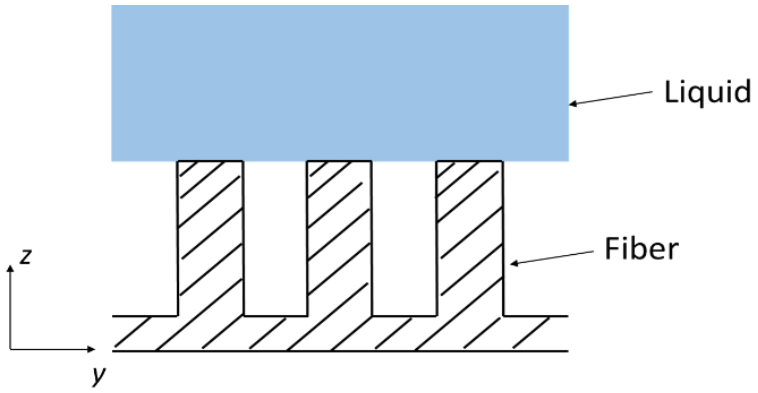

(a)

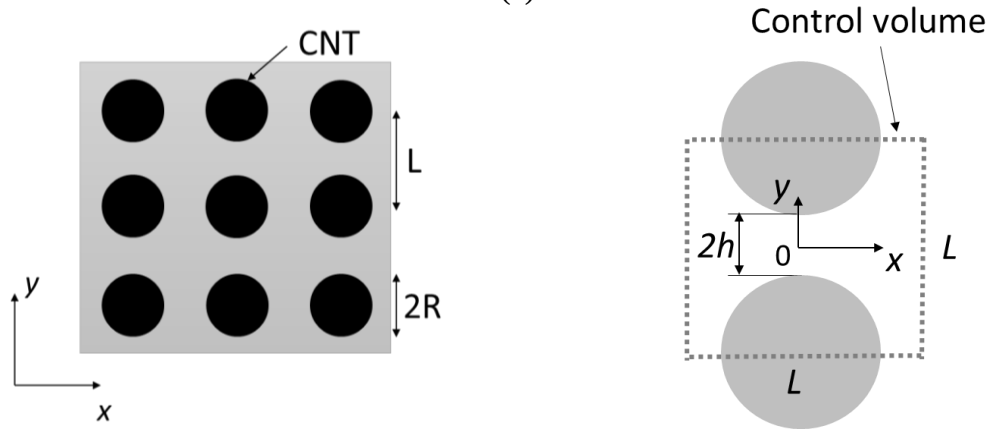

(b) (c)

Fig. 2 (a) is side view of and (b) is top view of schematics of the liquid interface in a surface with two-dimensional patterning with hydrophobic posts organized on a square lattice. (c) is definition of control volume.

Excerpt from ISBN 978-3-00-053387-7

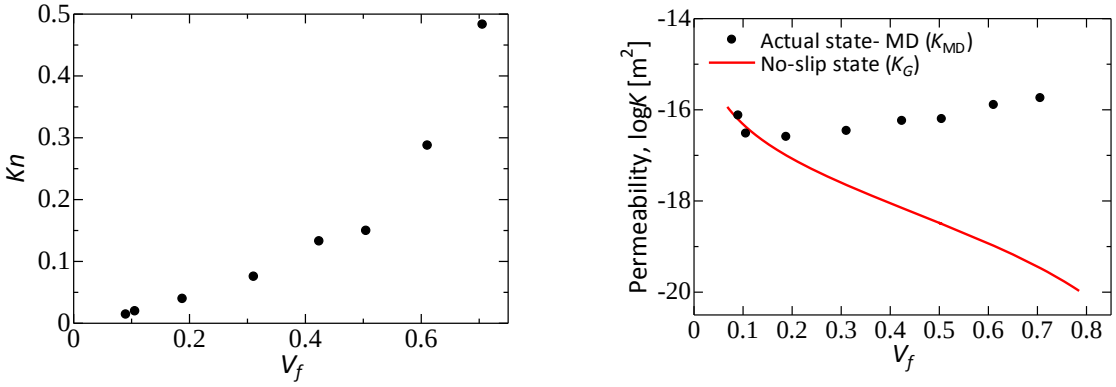

(a) (b)

Fig. 3 Diameter vs (a) *Kn* and (b) permeability.

Tables

Table 1. Parameters of AMBER96 potential function. *i*, *j*, and *k* represent an atom.

Atoms(*ij*)	ε_{ij} [kcal/mol]	σ_{ij} [Å]
CC	0.086	3.407
OO	0.1521	3.151
HH	0.0	0.0
CO	0.114	3.275
CH	0.0	0.0
Bonds(*ij*)	K_{ij}^R [kcal/mol/Å^2]	R_{ij}^{eq} [Å^2]
OH	1000.0	1.0
Angles(*ijk*)	K_{ijk}^θ [kcal/mol/rad^2]	θ_{ijk}^{eq} [°]
HOH	1,000.0	109.47

Table 2. Computational condition of simulation.

Relaxation	Time step [fs]	0.01
	Running time [fs]	20
	Damping constant	100.0
Simulation	Time step [fs]	1.0
	Running time [fs]	8.0×10^5
	Temperature [K]	300

Excerpt from ISBN 978-3-00-053387-7

References

[1] Y. Takeo, H. Yuhei, Y. Yuki, Y. Yoshiki, I. Ali, N. F. Don, and H. Kenji. A stretchable carbon nanotube strain sensor for human-motion detection. *Nature Nanotechnology*, 6:296-301, 2011.

[2] L. Ali, Y. Satoshi, K. Kazufumi, Y. Takeo, N. F. Don, H. Hiroaki, Y. Motoo, I. Sumio, and H. Kenji. Extracting the full potential of single-walled carbon nanotubes as durable supercapacitor electrodes operable at 4 V with high power and energy density. *Advanced Materials*, 22:E235-E241, 2010.

[3] C. Vitaly. Filling carbon nanotubes with liquid acetonitrile. *Chemical Physics Letters*, 496:50-55, 2010.

[4] S. Nuno, F. Bruno, and N. C. L. Jose. Compressive behavior of CNT-reinforced aluminum composites using molecular dynamics. *Composites Science and Technology*, 90:16-24, 2014.

[5] S. Yoshinobu, O. Kahori, T. Keiichiro, F. Tomoyuki, S. Keiichi, Y. Go, H. Toshiyuki, G. Ken, O. Toshio, N. Kimiyoshi, N. Takayuki, and L. Yoku. Tensile mechanical properties of carbon nanotube/epoxy composite fabricated by pultrusion of carbon nanotube spun yarn preform. *Composite: Part A*, 62:32-38, 2014.

[6] M. Grujicic, Y. P. Sun, and K. L. Koudela. The effect of covalent functionalization of carbon nanotube reinforcements on the atomic-level mechanical properties of poly-vinyl-ester-epoxy. *Applied Surface Science*, 253:3009-3021, 2007.

[7] X. Zhengtao, W. Xia, X. Xue, Z. Hong, L. Yan, and W. Yonghua. Base- and structure-dependent DNA dinucleotide-Carbon nanotube interactions: Molecular dynamics simulations and thermodynamic analysis. *The Journal of Physical Chemistry*, 115:21546-21558, 2011.

[8] S. Xinghua, V. D. B. Annette, H. H. Robert, B. K. Agnes, and G. Huajian. Cell entry of one-dimensional nanomaterials occurs by tip recognition and rotation. *Nature Nanotechnology*, 6:714-719, 2011.

[9] P. R. Jessica, F. C. Mark, R. B. Arnold, K. S. Jeanette, I. E. Jeffrey, W. T. Earl, R. M. Owen, A. W. Brian, E. D. Darol, E. A. Melvin, and C. Bonner. Inhaledz carbon nanotubes reach the subpleural tissue in mice. *Nature Nanotechnology*, 4:747-751, 2009.

[10] H. Kenji, D. N. Futaba, M. Kohei, N. Tatsunori, M. Yumura, and I. Sumio. Water-assisted highly efficient synthesis of impurity-free single-walled carbon nanotubes. *Science*, 306:1362-1364, 2004.

[11] S. Abdalla, F. Al-Marzouki, A. A. Al-Ghamdi, and A. Abdel-Daiem. Different technical applications of carbon nanotubes. *Nanoscale Research Letters*, 10:358, 2015.

[12] J. S. Babu, and S. P. Sathian. The role of activation energy and reduced viscosity on the enhancement of water flow through carbon nanotubes. *The Journal of Chemical Physics*, 134:194509, 2011.

[13] M. S. Dresselhaus, G. Dresselhaus, R. Saito, and A. Jorio. Raman spectroscopy of carbon nanotubes. *Physics Reports*, 409:47-99, 2005.

[14] F. Villalpando, H. Son, D. Nezich, Y. P. Hsieh, J. Kong, Y. A. Kim, D. Shimamoto, T. Muramatsu, T. Hayashi, M. Endo, M. Terrones, and M. S. Dresselhaus. Raman spectroscopy study of isolated double-walled carbon nanotubes with different metallic and semiconducting configurations. *Nano Letters*, 8:3870-3886, 2008.

[15] J. A. Thomas, and A. J. H. Mcgaughey. Reassessing fast water transport through carbon nanotubes. *Nano Letters*, 8:2788-2793, 2008.

[16] J. A. Thomas, and A. J. H. Mcgaughey. Water flow in carbon nanotubes: Transition to subcontinuum transport. *Physical Review Letters*, 102:184502, 2009.

[17] S. Joseph, and N. R. Aluru. Why are carbon nanotubes fast transporters of water? , *Nano Letters*, 8:452-458, 2008.

Excerpt from ISBN 978-3-00-053387-7

[18] J. Su, and H. Guo. Effect of nanochannel dimension on the transport of water molecules. *The Journal of Physical Chemistry*, 116:5925-5932, 2012.

[19] J. H. Walther, K. Ritos, R. C. Eduardo, C. M. Megaridis, and P. Koumoutsakos. Barriers to superfast water transport in carbon nanotubes membranes. *Nano Letters*, 13:1910-1914, 2013.

[20] J. K. Holt, H. G. Park, Y. Wang, M. Stadermann, A. B. Artyukhin, C. P. Grigoropoulos, A. Noy, and O. Bakajin. Fast mass transport through sub-2-nanometer carbon nanotubes. *Science*, 312:1034-1037, 2006.

[21] M. Majumder, N. Chopra, R. Andrews, and B. Hinds. Nanoscale hydrodynamics: enhanced flow in carbon nanotubes. *Nature*, 438:44, 2005.

[22] M. Majumder, N. Chopra, and B. J. Hinds. Mass transport through carbon nanotube membranes in three different regimes: Ionic diffusion and gas and liquid flow. *ACS Nano*, 5:3867-3877, 2011.

[23] X. Qin, Q. Yuan, Y. Zhao, S. Xie, and Z. Liu. Measurement of the rate of water translocation through carbon nanotubes. *Nano Letters*, 11:2173-2177, 2011.

[24] M. Whitby, L. Cagnon, M. Thanou, and N. Quirke. Enhanced fluid flow through nanoscale carbon pipes. *Nano Letters*, 8:2632-2637, 2008.

[25] L. Byeongho, Y. Baek, M. Lee, D. H. Jeong, H. H. Lee, J. Yoon, and Y. H. Kim. A carbon nanotube wall membrane for water treatment. *Nature Communications*, 6:7109, 2015.

[26] B. R. Gebart. Permeability of unidirectional reinforcements for RTM. *Journal of Composite Materials*, 26:1100-1133, 1992.

[27] L. Joly. Capillary filling with giant liquid/solid: Dynamics of water uptake by carbon nanotubes. *The Journal of Chemical Physics*, 135:214705, 2011.

[28] S. Wang, D. Haldane, R. Liang, J. Smithyman, C. Zhang, and B. Wang. Nanoscale infiltration behavior and through-thickness permeability of carbon nanotube buckypapers. *Nanotechnology*, 24:015704, 2013.

[29] L. Wang. Molecular dynamics-Studies of synthetic and biological macromolecules. *Intech Journals*, 2012.

[30] W. L. Jorgensen, J. Chandrasekhar, J. D. Madura, R. W. Impey, and M. L. Klein, Comparison of simple potential functions for simulating liquid water. *The Journal of chemical physics*, 79:926-935, 1983.

[31] M. A. González, and J. L. Abascal. The shear viscosity of rigid water models, *The Journal of Chemical Physics*, 132:096101, 2010.

[32] W. D. Cornell, P. Cieplak, C. L. Bayly, I. R. Gould, K. M. Merz, D. M. Ferguson, D. C. Spellmeyer, T. Fox, J. W. Caldwell, and P. A. Kollman. A second generation force field for the simulation of proteins, nucleic acids, and organic molecules. *Journal of the American Chemical Society*, 117:5179-5197, 1995.

[33] Y. Kohji. PPPM and TreePM methods on GRAPE systems for cosmological N-body simulations, *Publications of the Astronomical Society of Japan*, 57:849-860, 2005.

[34] H. C. Andersen. Rattle: A "velocity" version of the shake algorithm for molecular dynamics calculations. *Journal of Computational Physics*, 52:24-34, 1983.

[35] N. G. Jensen, and O. Faragol. A simple and effective verlet-type algorithm for simulating Langevin dynamics. *Molecular Physics*, 111:983-991, 2013.

[36] A. P. Thompson, S. J. Plimpton, and W. Mattson. General formulation of pressure and stress tensor for arbitrary many-body interaction potentials under periodic boundary conditions. *The Journal of Chemical Physics*, 131:154107, 2009.

[37] D. R. Willis. Sphere drag at high Knudsen Number and low Mach number, *Physics of Fluids*, 9:2522, 1966.

Excerpt from ISBN 978-3-00-053387-7